Building Tomorrow's Society

Bâtir la Société de Demain

Fredericton, Canada

June 13 – June 16, 2018/ *Juin 13 – Juin 16, 2018*

DESIGN CONSIDERATIONS FOR GLULAM BEAMS AND COLUMNS UNDER HIGH STRAIN-RATES

Lacroix, Daniel[1,3], Viau, Christian[2] and Doudak, Ghasan[2]

[1] Carleton University, Canada

[2] University of Ottawa, Canada

[3] Daniel.Lacroix2@Carleton.ca

Abstract: An experimental program investigating the behaviour of glulam beams and columns under high strain rates subjected to simulated blast loading was undertaken. Key observations from the full-scale tests such as the dynamic increase factor (DIF) and failure modes are presented in this paper. A DIF of 1.14 was found to be present only in the absence of continuous or closely aligned finger-joints (FJs) in the outer tension laminations. No increase was observed when continuous or closely aligned FJs were present. The behaviour was observed to be linear-elastic with no significant post-peak capacity. Also, no DIF was observed on the stiffness of the glulam members. A more refined approach using moment-curvature analysis and incorporating second-order effects in the design resistance curve yielded a more reasonable match with the actual behaviour of the glulam beam and column elements.

1 INTRODUCTION

Glulam consists of two or more layers of dimensional lumber joined together with glue and finger-joints (FJs) in the parallel-to-grain direction and is primarily used as beams and columns in the construction of larger wood structures. The layers are stress-rated, thereby allowing for tighter control on the individual lamination properties. A change in regulations permitting the construction of mid- to high-rise structures using wood (NRC 2015) combined with advancement in manufacturing technologies to produce high-performing engineered wood products (EWPs) has allowed wood to be utilized beyond the traditional low-rise light-frame structures and to become a viable material option for much larger structures.

Numerous research studies dealing with the effect of blast loads on the behaviour of light-frame wood structures have been undertaken, where expressions for the dynamic increase factor (DIF) for lumber studs (Jacques et al. 2014) and light-frame wood stud walls (Lacroix and Doudak 2015, Viau and Doudak 2016a, Viau and Doudak 2016b, Viau et al. 2016) were developed. Viau and Doudak (2016b) investigated the effect of realistic boundary conditions on the response of light-frame walls with typical and enhanced connection detailing. Research has also been conducted on the retrofitting of stud walls where enhancements of typical light-frame wall construction and connections were provided (Lacroix et al. 2014, Syron 2010, Viau and Doudak 2016b). While the aforementioned research contributed to the field of blast loading on wood structures, the studies primarily focused on the behaviour of light-frame structures using dimensional lumber. Relatively little research has been conducted on establishing the behaviour of heavy timber and EWPs subjected to blast loading. Thus far, research has been limited to the experimental investigation of strain-rate effects and failure modes of cross-laminated-timber (CLT) panels (Poulin et al. 2018) and glued laminated timber beams and columns (Lacroix 2017).

Taller wood structures are accompanied by an increase in gravity loads acting on the supporting members of lower stories of the building necessitating consideration for the effects of combined lateral-blast and axial gravity loads. To the authors' knowledge, prior to the current research program, no dynamic tests have been conducted on the response of glulam subjected to the effects of the combined lateral-blast and axial gravity loading.

The current paper presents key findings from the experimental program and provides design and analysis methodologies for glulam beam-columns subjected to simulated blast loading. Presented herein are the strain-rate effects, which were quantified by comparing the dynamic to static test results, and the implications of the observed dynamic failure mode on the DIF. More specifically, the focus of this paper is on the effects of variable axial load on the dynamic behaviour. The importance of key parameters and their impact on the response of columns is also discussed.

2 EXPERIMENTAL PROGRAM AND RESULTS

2.1 Experimental Program

Full-scale static and dynamic tests with and without axial load have been conducted with the objective to establish the flexural behaviour of glulam beams and columns as well as to validate a proposed predictive model. A suggested design approach is discussed and validated by comparing the methodology to results obtained from the experimental research program.

2.1.1 Material Description

The experimental program involves the testing of forty-four glulam specimens, statically and dynamically, under four-point bending. The glulam specimens investigated in this research program were obtained from two different manufacturers in which three different cross-sections were considered. The specimens' dimensions and grade consisted of 80 x 228 x 2,500 mm^3 Spruce-Pine (SP), 86 x 318 x 2,500 mm^3 24f-ES SP, and 137 x 222 x 2,500 mm^3 24f-ES SP. The nomenclature of the specimens is such that the letters (B or C) refer to the member type (beam or column) followed by the specimen number. The number in square brackets indicates the width of the narrow face of the cross-section. For example, B3-[86] refers to beam specimen number 3 with dimensions 86 x 318 x 2,500 mm^3 and grade 24f-ES. In addition to having multiple laminations composing the depth of the members, the width of the specimens investigated consisted of either a single laminate (e.g. 80 x 228 mm^2) or multiple laminates (e.g. 86 x 318 mm^2, 137 x 222 mm^2). The specimens with multiple laminates in the beam's width may consist of closely aligning FJs, which, as will be discussed later, has a significant effect on their behaviour. Throughout the paper, the term "beam" is used to describe specimens that have no axial load while being subjected to out-of-plane loading, whereas specimens subjected to combined axial and out-of-plane loads are referred to as "column".

2.1.2 Test Apparatuses and Instrumentation

The static tests were conducted using a four-point bending setup consisting of a reaction frame, hydraulic jack, and steel I-beam, in accordance with ASTM D198 (2015). Using load cells, wire gauges, and strain gauges, the time histories of the static reactions, mid-span displacement, and tensile and compressive wood strains were recorded with a data acquisition system at a sampling rate of 10 samples per second. The dynamic test setup (Fig. 1) closely mimicked the conditions of the static setup. The shock wave resulting from the release of the air in the driver section of the Shock Tube was transferred to the third points of the specimens using a load transfer device (LTD) covering the 2,032 x 2,032 mm^2 end frame opening. The LTD was able to freely displace up to 200 mm due to the slotted hinge system. Axial load was applied using two hydraulic jacks placed between the floor slab and bottom of the specimen whereas load cells measuring the axial load time history were placed at the top end of the specimen. The recorded output for the dynamic tests consisted of time histories for the reflected pressure, displacement, strain, reactions, and axial load. The sensors were connected to a data acquisition system recording at a sampling rate of 100,000 samples per second.

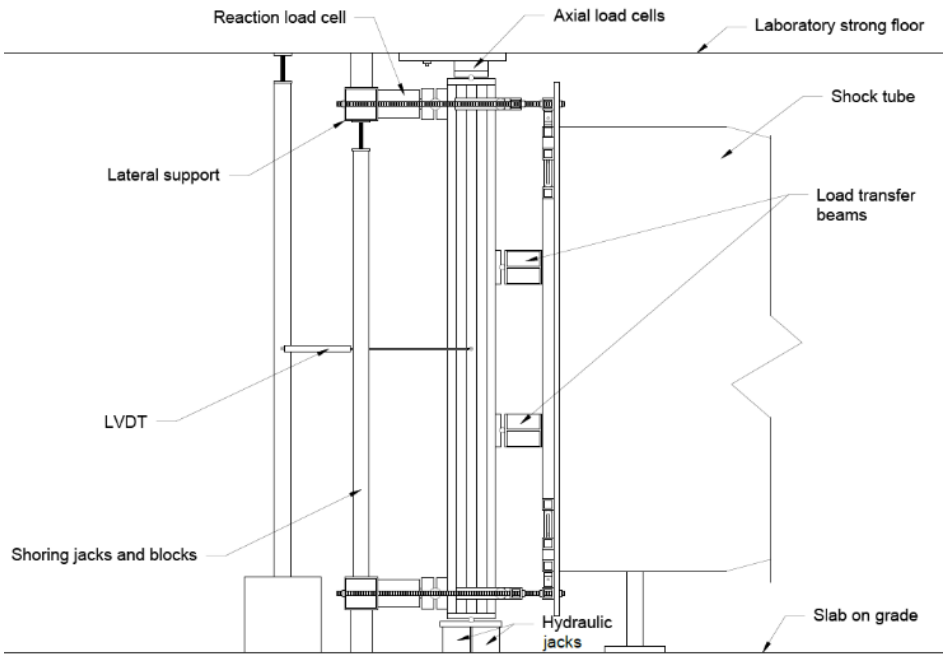

Figure 1: Dynamic test setup for columns

2.2 Full-Scale Test Analysis and Results

2.2.1 Characterization of Failure Modes

Figure 2 shows representative static and dynamic failure modes. During the static testing, the failure modes were limited to simple or splintering tension failure with initial failure occurring either at a knot or FJ (Fig. 2a) followed by propagation of cracks along the glulam layers. For beams with multiple laminates, for which the FJs were not closely aligned, the failure on the tension side appeared to be staggered (Fig. 2b) in comparison to the straight cut across the member width for beams with single laminate or closely aligned FJs across the beam width.

(a) B7-[80] (b) B4-[137] (c) B21.1-[80] (d) B8.2-[137] (e) C4.1-[137]

Figure 2: Representative static and dynamic failure modes

A brash tension failure occurred under dynamic loading for single laminate width beams (Fig. 2c) in comparison to the simple or splintering tension failure under static loading. It was also observed that specimens that had the presence of a FJ in the outer tension lamination within the two load points consistently failed at the FJ (Fig. 2c). Beams with multiple laminates across the member's width generally experienced significantly more crack propagation and splintering (Fig. 2d) than those observed during static testing. For the columns, the damage was concentrated near the member midspan with significant compression failure as evidenced by the wrinkling of the fibres (Fig. 2e).

2.2.2 Strain-Rate Effects – Dynamic Increase Factor (DIF)

Key results describing the average properties for each group of beams investigated including the modulus of elasticity (MOE), modulus of rupture (MOR), and tensile rupture strain ($\varepsilon_{f\text{-}T}$) are presented in Table 1 along with the coefficient of variation (COV). Strain-rates, defined as the strain at yield divided by the time at yield, varied between 0.14 – 0.51s^{-1}.

Table 1: Summary of beams' static and dynamic properties

Specimen group	Property	Static		Dynamic	
		Average	COV	Average	COV
B-[80]	MOE (MPa)	8,368	0.04	9,551	0.12
	MOR (MPa)	51.2	0.09	53.5	0.10
	$\varepsilon_{f\text{-}T}$ x 10^{-4} (mm/mm)	46.3	0.10	45.2	0.26
B-[86]	MOE (MPa)	8,025	0.04	7,807	0.05
	MOR (MPa)	41.5	0.03	46.8	0.20
	$\varepsilon_{f\text{-}T}$ x 10^{-4} (mm/mm)	36.0	0.05	35.8	0.19
B-[137]	MOE (MPa)	10,073	0.05	9,313	0.03
	MOR (MPa)	45.6	0.08	48.8	0.11
	$\varepsilon_{f\text{-}T}$ x 10^{-4} (mm/mm)	40.8	0.20	36.0	0.20

The MOE and MOR presented in Table 1 are “apparent material properties” based on the global response of the beams and were obtained using classical beam equations for the case of a simply supported beam with two concentrated loads at the span’s third points (Biggs 1964). Additional steps in obtaining the dynamic MOR and MOE were necessary, where the dynamic resistance was obtained using a single-degree-of-freedom approach considering the inertia effects of both the LTD and glulam specimen in the dynamic equilibrium (Jacques 2016, Lacroix 2017). Determining an average DIF for glulam beams should simply be a matter of relating the dynamic MOR of each glulam beam to the static average for the same type of beam, however, significant difference in the DIF values was observed depending on the failure mode.

Comparisons based on statistical analysis, involving the grouping of specimens by failure (e.g. continuous and staggered) and loading type (e.g. static and dynamic), yielded a DIF of 1.14 for specimens with staggered FJs or no continuous FJ (single width laminate beams) in the outer tension laminations within the maximum stress region (Lacroix 2017). No significant difference was observed between the static and dynamic specimens with a continuous failure indicating that specimens with continuous failure lack the increase associated with high strain-rates. Similar analyses were conducted by the authors for the modulus of elasticity and failure strain, however, the results showed no evidence of a dynamic increase (Lacroix 2017).

2.3 Effect of Axial Load

The effect of axial load was investigated by testing six columns with three different axial load ratios (ALRs). Figures 3a and 3b show representative data for C3-[137] obtained from the column tests. From Figure 3a it can be seen that although the column returned to initial position it experienced some level of damage as indicated by the sudden drop in tensile strain. A comparison of the time at which tensile failure occurred (Fig. 3a) to the peak dynamic reaction (Fig. 3b) shows that both occurred approximately at the same time. A loss in axial load was observed throughout the response of the columns (Fig. 3c), which is consistent with previous findings (e.g. Kadhom 2015, Lloyd 2015). However, the magnitude of the axial load corresponding to peak resistance was more significant (ranging from 50 to 83% of the initial load) than that reported elsewhere for reinforced concrete columns (e.g. Lloyd 2015). Since the span was similar to the aforementioned studies, the difference can be attributed to the compressive stiffness of the glulam columns being significantly less than that of concrete. The dynamic resistance of the column, $R_r(y,t)$, shown in Figure 3c was obtained using Equation 1:

[1] $$R_r(y,t) = R(y,t) - \frac{6P_a(t)}{L} y(t)$$

where $R(y,t)$ is the dynamic resistance if there were no axial load, $P_a(t)$ is the experimentally measured axial load time history, $y(t)$ is the midspan deflection of the column as a function of time, and L is the clear span. Because the measured dynamic reactions do not account for the secondary moments, an equivalent lateral load (ELL) reflecting the spatial distribution of the blast load (e.g. four-point bending) with the same magnitude as the secondary moments was used.

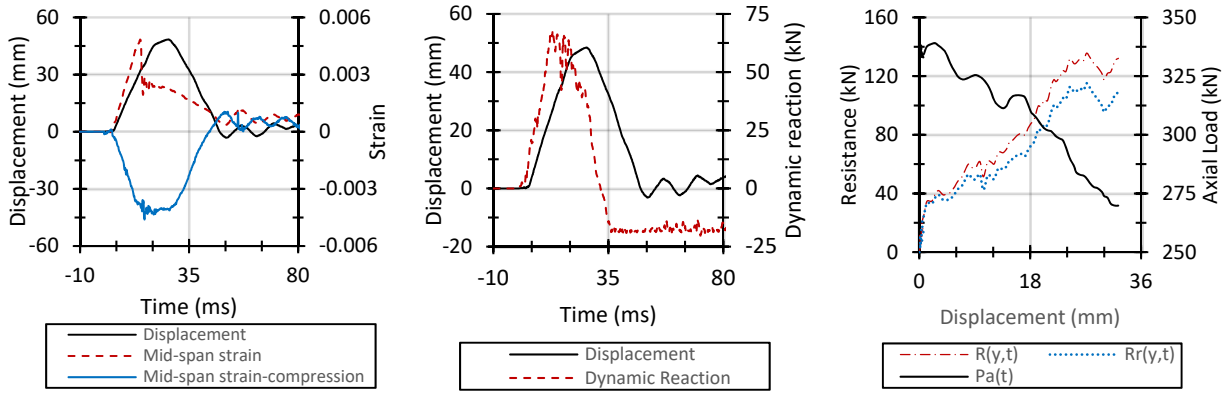

(a) Displacement and strain (b) Displacement and reaction (c) Resistance and axial load

Figure 3: Representative data for C3.1-[137]

It was observed that the addition of axial load has, on average, resulted in a displacement at maximum resistance and a tensile failure strain that are 1.05 and 1.26 times, respectively, greater than those attained in the beam specimens tested dynamically.

3 DESIGN CONSIDERATIONS FOR GLULAM BEAMS AND COLUMNS

3.1 Current CSA S850 Design Approach

Guidance on how to obtain the dynamic design strength of structural components based on the specified static strength is provided in the Canadian blast design standard (CSA 2012). The accuracy of the resistance curve to be used in the dynamic analysis is highly influenced by the assumptions and input parameters for the model. The following investigates the effects of the Canadian blast standard design assumptions on the prediction of the dynamic flexural resistance curves for the B-[137] beams. The resistance and stiffness for a simply supported beam under four-point bending can be found using Equations 2 and 3, respectively:

[2] $R_e = \frac{6S_D}{\mathrm{L}}$

[3] $\mathrm{K} = \frac{56.4\ \mathrm{EI}}{5L^3}$

where R_e is the yield resistance, S_D the dynamic design strength, K the stiffness, E the elastic modulus, and I the moment of inertia. The yield point (x_e) can be found using Equation 4.

[4] $\mathrm{x_e} = \frac{\mathrm{R_e}}{\mathrm{K}}$

The dynamic design strength, shown in Equation 2, is obtained by amplifying the specified static strength (S_S) by a dynamic increase factor (*DIF*) and strength increase factor (*SIF*) as shown in Equation 5.

[5] $\mathrm{S_D} = \mathrm{DIF} * \mathrm{SIF} * \mathrm{S_S}$

The DIF and SIF for glulam suggested by the blast standard (CSA 2012) are 1.4 and 1.2, respectively, whereas the specified static strength, S_s, is determined according to the timber design standard (CSA 2014) as shown in Equation 6.

[6] $S_s = \min\{\varphi[f_b(K_D K_H K_{Sb} K_T)]SK_X K_L;\ \varphi[f_b(K_D K_H K_{Sb} K_T)]SK_X K_{Zbg}\}$

where φ is the material resistance factor, f_b is the bending strength, K_D is the load duration factor, K_H is the system factor, K_{Sb} is the service condition factor for bending at extreme fiber, K_T is the treatment factor, S is the section modulus, K_X is the curvature factor, K_L is the lateral stability factor, and K_{Zbg} is the size factor.

The design assumptions provided by the blast standard (CSA 2012) were investigated and compared to both the experimentally determined dynamic resistance curves and the proposed design approach for glulam beams. The two key parameters investigated are the DIF and response limits. Currently, the blast standard (CSA 2012) assigns a DIF of 1.4 for glulam while the response limits for flexure vary from ductility ratios of 1 through 4 corresponding to increasing damage levels representing elastic to blowout, respectively.

The material resistance factor (φ) is assumed to be equal to unity mainly due to the uncertainties and rarity of occurrence of loading (CSA 2012). The load duration factor K_D is also taken as unity in blast design (CSA 2012). The service factor in bending, treatment factor, curvature factor, and lateral stability factor are all taken as unity to reflect the test conditions, whereas the size factor was taken as 1.3 in conformance with the timber design provisions (CSA 2014). The bending strength was taken as 30.7 MPa based on published data while the modulus of elasticity was taken as the average experimental MOE shown in Table 1. To provide a meaningful comparison with experimental results, the SIF derived from the experimental results was used. The value is reflective of the particular specimens tested and as such, the authors are not suggesting to modify the value existing in the blast design standard.

The flexural resistance resulting from the code design approach is shown in Figure 4 along with the experimental dynamic resistance curves for the B-[137] beams. It can be seen that using a DIF of 1.4 over-predicts the dynamic resistance of the beams. Also, it can be seen that using a perfectly linear elastic-plastic resistance curve with a ductility ratio of 4 is not reflective of the actual glulam beams' behaviour. The beams are observed to behave linearly up to peak resistance followed a significant drop in resistance providing little to no additional energy dissipation.

Also shown in Figure 4 is the flexural resistance curve obtained using the proposed design approach which consists of using a DIF of 1.14 with a linear-elastic resistance curve due to the lack of post-peak resistance (Lacroix 2017). It can be seen that the proposed design approach is more reflective of the actual behaviour of the beams.

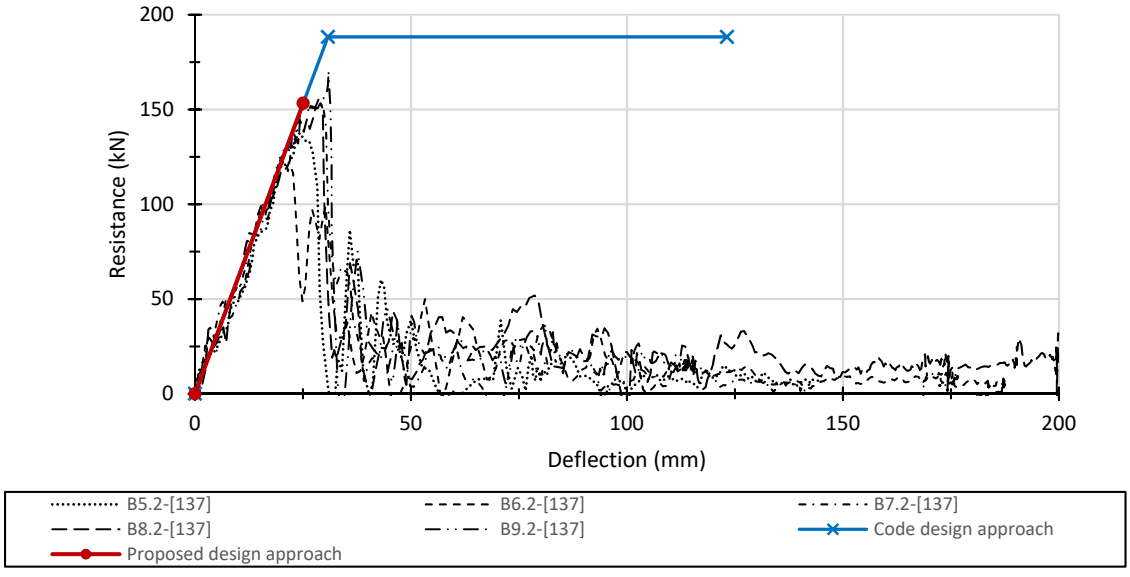

Figure 4: Resistance curves generated from code approach

3.2 Effect of Axial Load

The columns' experimental resistance curves were determined using the ELL approach together with experimentally determined inputs (i.e. dynamic reaction-, applied pressure-, and axial load-time histories) and were shown to corroborate well with the predicted behaviour from the moment-curvature analysis (Lacroix 2017). A material model using tensile and compressive wood stress-strain relationship (determined experimentally) was developed and composite resistance curves were generated to capture the observed loss in axial load. Further details on how the material model and composite resistance curves were developed can be found in Lacroix (2017).

The discussion herein focuses on the effect of varying the axial load with the following hypothetical case. The column is assumed to have the following material properties: ε_{tf} = 0.0045 mm/mm, E_{Wc} = 10,000 MPa, f_{cy} = 35 MPa, and ε_{cult} = 0.014 mm/mm. Figures 5 to 8 present the results from the sensitivity analysis for the following six cases: Case 1 – $E_{Wt} = E_{Wc}$; $m = 0.01$, Case 2 – $E_{Wt} = E_{Wc}$; $m = 0.2$, Case 3 – $E_{Wt} = 2E_{Wc}$; $m = 0.01$, Case 4 – $E_{Wt} = 2E_{Wc}$; $m = 0.2$, Case 5 – $E_{Wt} = 0.5E_{Wc}$; $m = 0.01$, and Case 6 – $E_{Wt} = 0.5E_{Wc}$; m = 0.2. The analyses were conducted for the 137 x 222 mm^2 cross-section with a span length of 2,235 mm. It should be noted that the resistance curves shown include the effect of the secondary moments and would be more prominent with increasing column length.

In general, the analysis revealed that for all six cases increasing the level of axial load resulted in a decrease in maximum moment and resistance, which is consistent with the observations made by Buchanan (1986) for the case $E_{Wt} = E_{Wc}$. This behaviour is at odds with the reported increase in stiffness and resistance observed with increasing compressive axial load for reinforced concrete columns (Burrell et al. 2015, Jacques et al. 2013, Lloyd 2015). It should be noted, however, that this behaviour depends on the stress-strain relationship used as input in the moment-curvature analysis. For example, when the tension MOE (E_{Wt}) is significantly higher than that of the compression MOE (E_{Wc}), a slight reduction in stiffness is observed as the levels of applied axial load increases (Figs. 5c, 6c, 7a, and 8a). This particular behaviour results in an increase in stiffness in the composite resistance curve as there is a loss of applied axial load. It can also be observed that while there is an increase in ultimate curvature due the applied axial load (Figs. 5a, 5b, 5c and 7a) it is not necessarily reflected in the resistance curves due to the secondary moments dominating the overall response (Figs. 6a, 6b, 6c and 8a) resulting in lower failure deflections.

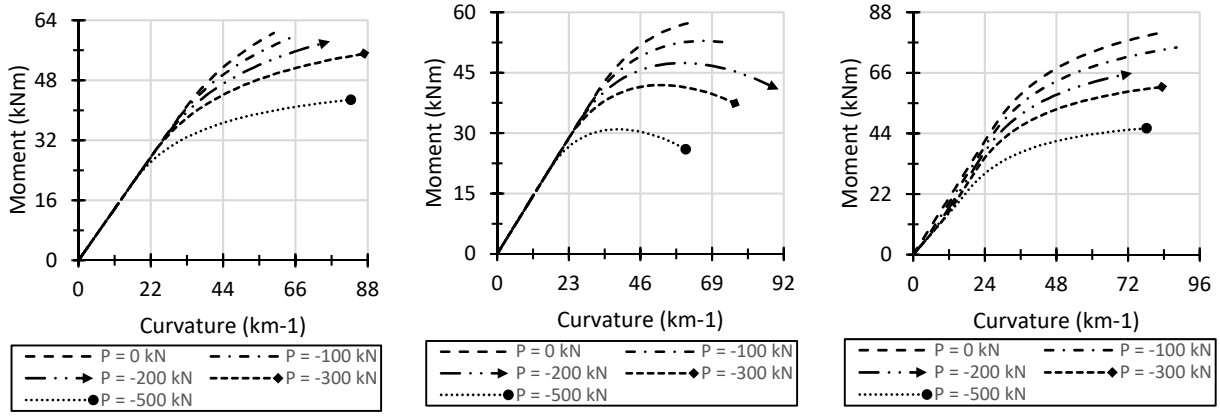

(a) Case 1 – $E_{Wt} = E_{Wc}$; $m = 0.01$ (b) Case 2 – $E_{Wt} = E_{Wc}$; $m = 0.2$ (c) Case 3 – $E_{Wt} = 2E_{Wc}$; $m = 0.01$

Figure 5: Moment-curvature for Cases 1 to 3

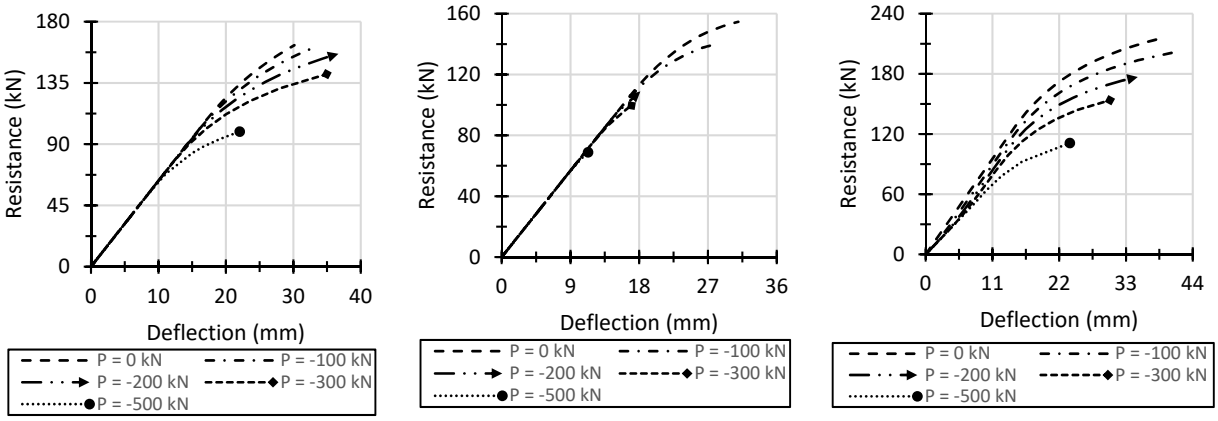

(a) Case 1 – $E_{Wt} = E_{Wc}$; $m = 0.01$ (b) Case 2 – $E_{Wt} = E_{Wc}$; $m = 0.2$ (c) Case 3 – $E_{Wt} = 2E_{Wc}$; $m = 0.01$

Figure 6: Resistance curves for Cases 1 to 3

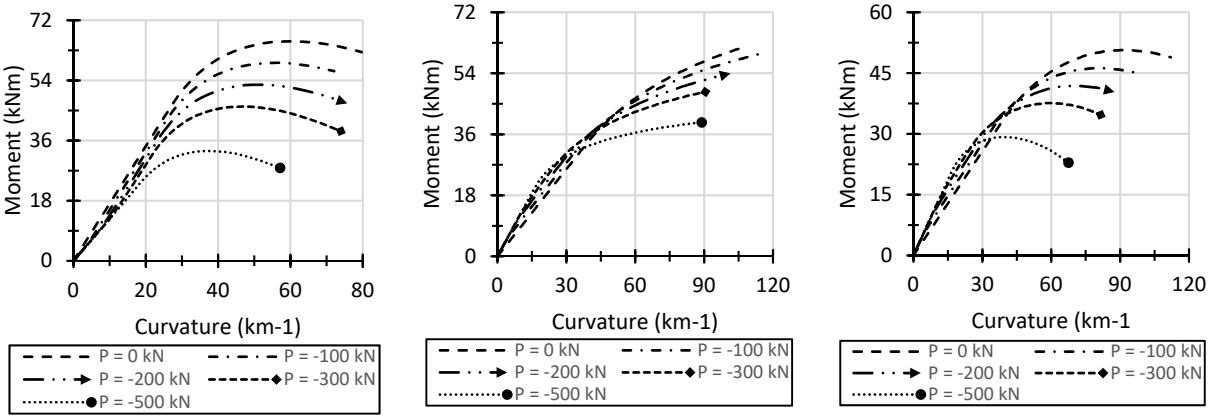

(a) Case 4 – $E_{Wt} = 2E_{Wc}$; $m = 0.2$ (b) Case 5 – $E_{Wt} = 0.5E_{Wc}$; $m = 0.01$ (c) Case 6 – $E_{Wt} = 0.5E_{Wc}$; $m = 0.2$

Figure 7: Moment-curvature for Cases 4 to 6

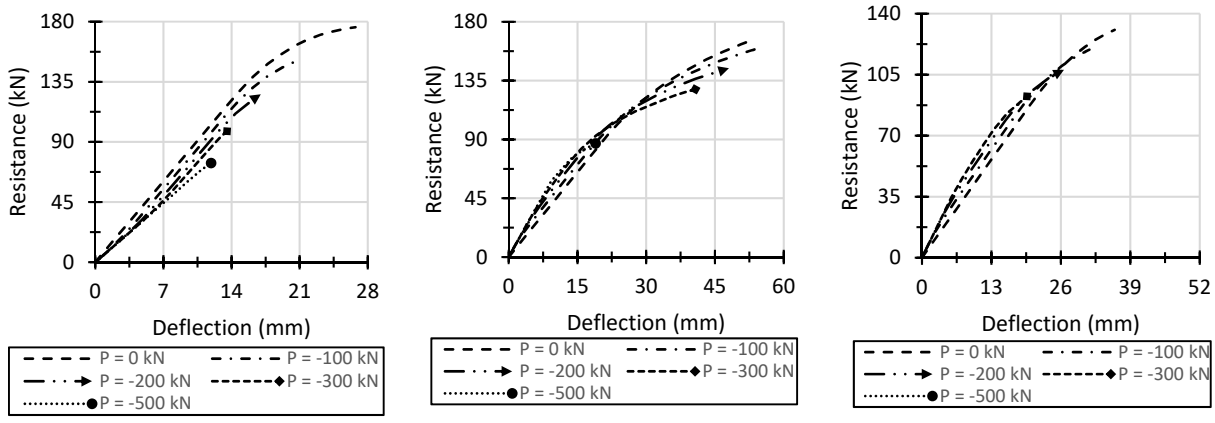

(a) Case 4 – $E_{Wt} = 2E_{Wc}$; $m = 0.2$

(b) Case 5 – $E_{Wt} = 0.5E_{Wc}$; $m = 0.01$

(c) Case 6 – $E_{Wt} = 0.5E_{Wc}$; m = 0.2

Figure 8: Resistance curves for Cases 4 to 6

For the case where E_{Wt} is significantly lower than E_{Wc} (e.g. Cases 5 and 6), there is an initial increase in stiffness with increasing applied axial load, thus resulting in a decrease in stiffness in the composite curve. Although there is an increase in stiffness due to increasing applied axial load, it should be noted that the ultimate moment with axial load is lower than the case of no axial load.

The analysis presented herein highlights the importance of using representative material properties when conducting moment-curvature analysis for wood due to the notable differences discussed. Although the ELL method was used to determine the experimental resistance curves, its use in design without nonlinear reaction-, axial load-, displacement-, and pressure-time histories should be cautioned. Simply applying the ELL method to the resistance curve of the case where there is no axial load may not capture key aspects of the behaviour such as increase in stiffness and increase or decrease in failure displacement. In terms of design approach, it is suggested that a moment-curvature be used to capture the non-linear effects resulting from the material properties and second-order effects. Furthermore, a ductility ratio of 1 should be used due to the lack of post-peak resistance observed in both the beams and columns.

4 CONCLUSIONS

Presented herein are the results of an experimental program investigating the behaviour of glulam beams and columns subjected to blast loading. The results have shown that a DIF of 1.14 is appropriate only when continuous or closely aligned FJs are not found in the outer tension lamination of the glulam specimen. No increase was observed when continuous or closely aligned FJs were present. The post-peak resistance of the glulam beams and columns was not observed to be significant and thus it is suggested that they be designed using a linear-elastic flexural resistance curve, thereby limiting the ductility ratio to unity. Further, no DIF on the stiffness should be applied. In dealing with axial loading, a more refined approach using moment-curvature and incorporating second-order effects should be employed to reflect the actual behaviour of the column.

References

ASTM. 2015. *Standard Test Methods of Static Tests of Lumber in Structural Sizes*. *ASTM D198-15*. West Conshohocken, PA, American Society for Testing and Materials.

Biggs, J.M. 1964. *Introduction to Structural Dynamics*. New York, NY: McGraw-Hill.

Buchanan, A., H. 1986. Combined bending and axial loading in lumber. *Journal of Structural Engineering*, **112**(12):18.
Burrell, R., Aoude, H., and Saatcioglu, M. 2015. Response of SFRC columns under blast loads. *Journal of Structural Engineering*, **141**(9).
CSA. 2012. Design and assessment of buildings subjected to blast loads. *CSA S850*. Mississauga, ON, Canadian Standards Association Group.
CSA. 2014. Engineering design in wood. *CSA O86*. Mississauga, ON, Canadian Standards Association Group.
Jacques, E. 2016. Characteristics of reinforced concrete bond at high strain rates. Ph.D., Civil Engineering, University of Ottawa.
Jacques, E., Lloyd, A., Braimah, A., Saatcioglu, M., Doudak, G., and Abdelalim, O. 2014. Influence of high strain-rates on the dynamic flexural material properties of spruce–pine–fir wood studs. *Canadian Journal of Civil Engineering*, **41**(1):56-64.
Jacques, E., Lloyd, A., and Saatcioglu, M. 2013. Predicting reinforced concrete response to blast loads. *Canadian Journal of Civil Engineering*, **40**(5):427-444.
Kadhom, B. 2015. Blast performance of reinforced concrete columns protected by FRP laminates. Ph.D., Civil Engineering, University of Ottawa.
Lacroix, D. 2017. Investigating the Behaviour of Glulam Beams and Columns Subjected to Simulated Blast Loading. Ph.D., Civil Engineering, University of Ottawa.
Lacroix, D.N., and Doudak, G. 2015. Investigation of Dynamic Increase Factors in Light-Frame Wood Stud Walls Subjected to Out-of-Plane Blast Loading. *Journal of Structural Engineering*, **141**(6):04014159.
Lacroix, D.N., Doudak, G., and El-Domiaty, K. 2014. Retrofit options for light-frame wood stud walls subjected to blast loading. *Journal of Structural Engineering*, **140**(4):8.
Lloyd, A. 2015. Blast retrofit of reinforced concrete columns. Ph.D., Civil Engineering, University of Ottawa.
NRC. 2015. National Building Code of Canada. Ottawa, National Research Council of Canada,.
Poulin, M., Viau, C., Lacroix, D.N., and Doudak, G. 2018. Experimental and Analytical Investigation of Cross-Laminated Timber Panels Subjected to Out-of-Plane Blast Loads. *Journal of Structural Engineering*, **144**(2):04017197.
Syron, W.D. 2010. Strain Rate-Dependent Behavior of Laminated Strand Lumber. University of Maine.
Viau, C., and Doudak, G. 2016a. Investigating the Behavior of Light-Frame Wood Stud Walls Subjected to Severe Blast Loading. *Journal of Structural Engineering*, **142**(12):04016138.
Viau, C., and Doudak, G. 2016b. Investigating the behaviour of typical and designed wall-to-floor connections in light-frame wood stud wall structures subjected to blast loading. *Canadian Journal of Civil Engineering*, **43**(6):562-572.
Viau, C., Lacroix, D.N., and Doudak, G. 2016. Damage level assessment of response limits in light-frame wood stud walls subjected to blast loading. *Canadian Journal of Civil Engineering*, **44**(2):11.